Journal Paper

"Smart Farming: Intelligent management approach for crop inspection and evaluation employing unmanned aerial vehicles"

- International Conference on Management Science and Engineering Management-

July 2020

Carlos Quiterio Gómez Muñoz
Universidad Europea de Madrid, Spain
Carlosquiterio.gomez@universidadeuropea.es

Christian Paredes Alvarez
Universidad Europea de Madrid, Spain

Fausto Pedro García Márquez
Ingenium Research Group, Universidad de Castilla-La Mancha
FaustoPedro.Garcia@uclm.es

Cite as: Muñoz, C. Q. G., Alvarez, C. P., & Marquez, F. P. G. (2020, July). Smart Farming: Intelligent Management Approach for Crop Inspection and Evaluation Employing Unmanned Aerial Vehicles. In International Conference on Management Science and Engineering Management (pp. 119-130). Springer, Cham.

Smart Farming: Intelligent management approach for crop inspection and evaluation employing unmanned aerial vehicles

Carlos Quiterio Gómez Muñoz[1], Christian Paredes[1], Fausto Pedro García Marquez[2]

[1] Universidad Europea de Madrid, Spain

Carlosquiterio.gomez@universidadeuropea.es

[2] Ingenium Research Group, Castilla-La Mancha University, Spain

FaustoPedro.Garcia@uclm.es

Abstract

This work presents an unmanned aerial vehicle management platform encompassed in the concept of smart farming. Automates inspections of different crops and monitors the status of the plantation is done by IoT, analyzing an area on an online map that provides air and weather restrictions. Intelligent route management algorithms are employed to generate the optimal inspection route and waypoints, maximizing the multispectral images capture. These multispectral images can be subsequently processed according to algorithms based on phytosanitary index formulas and regressions obtained with artificial neural networks. Reports are generated with analysis of the results by this approach, for example: optimal collection time, water stress, maturity index, etc.

Keywords: Smart Farming, non-destructive tests, crop evaluation, route management, multispectral images, unmanned aerial vehicles.

1. Introduction

Agriculture is an essential sector for the economy, and it also affects the environment [1]. The sustainable economy is based mainly in sustainable agriculture [2]. The sector is moving towards specialization and an important technological development due to competitiveness at international level, the restrictions of water reserves, the needs of intensification of production and the adaptation to an increasingly restrictive environmental regulation.

A sustainable economy model agriculture should consider new technologies that allow an efficient use of increasingly scarce resources to minimize the environmental cost, and at the same time to meet the needs of the population [3]. It requires to optimize the production while developing healthy ecosystems and supporting the sustainable management of land, water and natural resources, guaranteeing the satisfaction of the needs of both present and future generations.

Within this context, precision agriculture is a fundamental part of sustainable agriculture and it is included in the called "Agriculture 4.0" [4,5]. It employs techniques for agri-food production that allow advantages of the available resources utilization, and avoid, or minimize, the production of toxic waste [6]. Precision agriculture allows to know where, how and when to apply the resources, and to obtain maximum benefits within a sustainable environment, knowing the current state of crops over the time.

In this context, it is essential to have as much information as possible about crop parameters in order to obtain decisions that improve the quality and efficiency of production [7,8]. This data collection is usually done with ground level sensors, sensors attached to the plants or through the acquisition of multispectral aerial images of the crop field~~or with aerial images of the crop field~~ [9]. Aerial images are images obtained with special cameras sensitive to narrow bands of the electromagnetic spectrum. With this information is possible to perform an analysis to know the status of the crops and have a solid basis for decision making [10,11]. It is optimized the use of scarce resources, distribute the necessary products locally and, according to the needs at each point, to minimize waste by the appropriate preventive and corrective actions in each case [12].

In order to perform this aerial work, it is important to calculate an optimal route for the unmanned aerial vehicles (UAV) [13,14]. Due to the technological limitations of UAVs, such as battery capacity, maximum flight time, etc., it requires optimal routes to maximize the number of multispectral image capture with each UAV flight [15,16].

Con formato: Sin Resaltar

Código de campo cambiado

Con formato: Resaltar

Código de campo cambiado

Código de campo cambiado

Código de campo cambiado

Código de campo cambiado

Código de campo cambiado

One of the main novelties of this paper regarding to other smart routes algorithms for UAVs is that it is specially designed for capturing multispectral images, which require to be captured in particular conditions to facilitate their subsequent processing [17]. The processing of these images, that usually have a low resolution, consists of joining them to generate a new larger image and facilitate the extraction of data from large regions. To perform these operations, it is necessary to set the same direction of the UAV in all waypoints. This direction will set the direction of the UAV advance and will generate a route composed of paths parallel to this direction. In addition, in order to facilitate its subsequent image processing, there will be an overlap of a certain percentage of common areas between captures of each waypoint.

2. Tessellation algorithm of a region and calculation of the optimal route for the UAV

The flight mission encompasses all the procedures that are part of the calculation of the parameters that will be sent to the UAVs [18,19], therefore, it finds the points from which it will capture hyperspectral images that will subsequently be processed and analysed to find vegetation indices [20].

It was defined two operations for the flight mission:

- Flight height and distance between image capture points.
- Calculation of spatial coordinates of image capture points.

It is sought to tessellate any polygonal area by means of rectangles of fixed dimensions, which covers its surface and a part of the surrounding surfaces. These rectangles are suitable for tessellation, since they cover a plane when assembled one after the other, without overlapping or leading spaces between them. It is possible to use this algorithm with other geometric figures, such as regular hexagons.

Given the n vertices of the closed and simply connected polygon that delimits the area to be explored, defined by its coordinates as the points $P_i = (x_i, y_i)$, where $i = 1,2,3 \ldots n$. Then, it is chosen the maximum and minimum coordinates on each axis to obtain a quadrilateral that surrounds and contains the polygon by equation (1):

$$x_{min} = min(xi), \quad x_{max} = max(xi), \quad y_{min} = min(yi), \; y_{max} = max(yi) \tag{1}$$

Four points are defined that will be the vertices of the rectangle that will contain the original polygon, according to equation (2):

Con formato: Color de fuente: Automático, Sin Resaltar
Código de campo cambiado
Con formato: Color de fuente: Automático, Sin Resaltar
Con formato: Color de fuente: Automático
Con formato: Sin Resaltar
Con formato: Sin Resaltar
Código de campo cambiado
Código de campo cambiado
Con formato: Sin Resaltar
Código de campo cambiado
Con formato: Sin Resaltar
Código de campo cambiado
Con formato: Sin Resaltar
Código de campo cambiado

$$P_{1r}=(x_{min},y_{min}) \quad P_{2r}=(x_{min},y_{max}) \tag{2}$$

$$P_{3r}=(x_{max},y_{max}) \quad P_{4r}=(x_{max},y_{min})$$

Figure 1~~Figure 1~~ shows the dimensions of the rectangle formed by these four points given by equation (3):

$$L_x = x_{max} - x_{min}; L_y = y_{max} - y_{min} \tag{3}$$

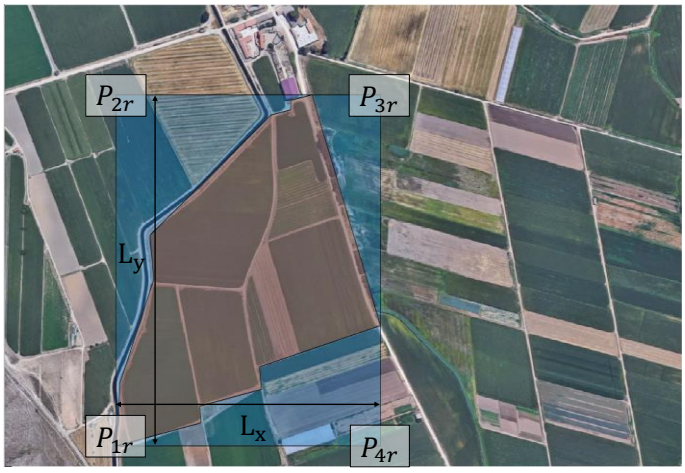

Figure 1. Satellite image to tessellate an area: The area to explore (orange); the rectangle that contains the orange zone (blue)

The dimensions on each axis of the polygon to test, and the distance between the barycenters of a polygon and the subsequent one in the tessellation, are defined. The dimensions of the rectangle are height a and base b , being the dimensions of the image to be captured by the camera. The vertical and horizontal distances between two centres of consecutive rectangles are a and b respectively.

The minimum safety margins for image capture are expressed based on the dimensions of the rectangle where the tessellation is performed, according to equation (4).

$$M_v = \%mv \cdot a \tag{4}$$

$$M_h = \%mh \cdot b$$

Código de campo cambiado
Con formato: Fuente: Sin Negrita
Código de campo cambiado
Con formato: Fuente: Sin Negrita, Sin Resaltar
Con formato: Sin Resaltar
Con formato: Sin Resaltar
Con formato: Sin Resaltar
Comentado [CQGM1]: Imagen actualizada y vectorizada
Con formato: Sin Resaltar
Con formato: Sin Resaltar
Con formato: Sin Resaltar
Con formato: Sin Resaltar
Código de campo cambiado
Con formato: Sin Resaltar
Con formato: Sin Resaltar
Código de campo cambiado
Código de campo cambiado
Con formato: Sin Resaltar
Código de campo cambiado
Con formato: Sin Resaltar
Con formato: Sin Resaltar
Con formato: Sin Resaltar
Con formato: Sin Resaltar

Where the M_v and M_h are the vertical and horizontal overlapping margins. The rectangle that contains the area to study is enlarged with these overlapping margins. The new vertices are given by equation (5).

$$P'_{1r}=(x_{min}-M_h, y_{min}-M_v) \quad P'_{2r}=(x_{min}-M_h, y_{max}+M_v)$$
$$P'_{3r}=(x_{max}+M_h, y_{max}+M_v) \quad P'_{4r}=(x_{max}+M_h, y_{min}-M_v) \tag{5}$$

The larger rectangle is divided into rectangles with the size of the image to bed captured, taking into account the overlapping margins by equation (6),

$$V = Ly + 2\cdot M_v; \quad m = \frac{V}{a} \tag{6}$$

$$H = Lx + 2\cdot M_h; \quad n = \frac{H}{b} \tag{7}$$

where n and m *are* integer values.

It is obtained that the number of rectangles, i.e. images, necessary for tessellation, is $n \times m$. To calculate the centre of each of them, the first point is defined by equation (8),

$$Q_1 = (Q_{1x}, \ Q_{1y}) \tag{8}$$

where

$$Q_{x1} = x_{min} - M_h + b \tag{9}$$

and

$$Q_{y1} = y_{min} - M_v + b \tag{10}$$

Equation (11) is employed to find the points matrix that determine the center of each of the rectangles that test the greater rectangle (Figure 2~~Figure 2~~),:

$$Q_{m\times n} = (x_{min} + j.b, \quad y_{min} + k.h); \quad Q = [Q_{mxn}] \tag{11}$$

being $j = 0,1,2\ldots n$ and $k = 0,1,2\ldots m$

Con formato: Sin Resaltar
Con formato: Sin Resaltar
Código de campo cambiado
Con formato: Sin Resaltar
Código de campo cambiado
Código de campo cambiado
Código de campo cambiado
Código de campo cambiado
Código de campo cambiado
Con formato: Sin Resaltar
Código de campo cambiado
Con formato: Sin Resaltar
Con formato: Sin Resaltar
Código de campo cambiado
Con formato: Sin Resaltar
Con formato: Sin Resaltar
Código de campo cambiado
Código de campo cambiado
Código de campo cambiado
Con formato: Fuente: Sin Negrita
Código de campo cambiado

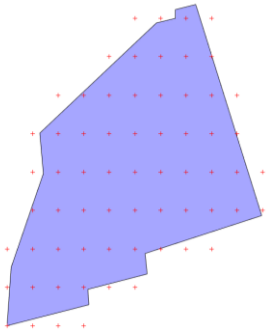

Figure 2 Points and rectangles of the area to be analysed.

A rectangle of size $a \times b$ is constructed from each of the generated points that will be the centers of each rectangles (Figure 3~~Figure 3~~). Its vertices are calculated by equation (12).

$$\mathbf{V}_{1i} = \left(Q_{xi} - \frac{b}{2}, Q_{yi} - \frac{a}{2} \right),\ \mathbf{V}_{2i} = \left(Q_{xi} - \frac{b}{2}, Q_{yi} + \frac{a}{2} \right)$$

$$\mathbf{V}_{3i} = \left(Q_{xi} + \frac{b}{2}, Q_{yi} + \frac{a}{2} \right),\ \mathbf{V}_{4i} = \left(Q_{xi} + \frac{b}{2}, Q_{yi} - \frac{a}{2} \right) \quad (12)$$

and

$$\mathbf{V}r = [\mathbf{V}_1\ \mathbf{V}_2\ \mathbf{V}_3\ \mathbf{V}_4\ ] \quad (13)$$

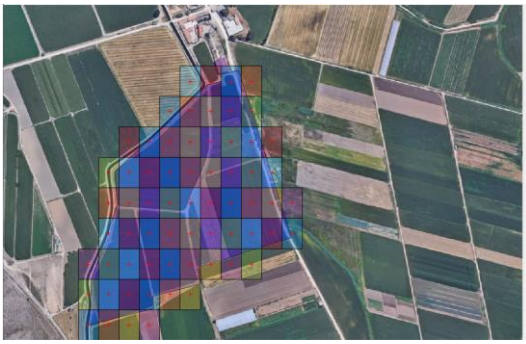

Figure 3. Tessellated area. Red dots indicate the position where the UAV should be located to make the image capture.

The rectangles that are totally or partially inside the polygon are checked to obtain the set of rectangles that make the tessellation of the original polygon. The approach verifies if at least one of the vertices is within the polygon and then, in this case, the rectangle belongs to the final tiling. The Ray Casting algorithm is used, which indicates that if an imaginary ray is thrown out of the point, and the number of intersections with the sides of the polygon is odd, the point is included in the polygon, otherwise it is outside the polygon ~~(straight line generation parallel to the axes from the point)~~ [21]. In addition, this method was validated with the dominant point method ~~, the dominant point (any point below and to the left of a point that does not belong to the selected area does not belong to the selected area)~~ [22]~~, are used etc.~~

When the rectangles are set as part of the tessellation, the $\boldsymbol{Q_t}$ matrix is done considering the ordered central points. These points, size a x b, define where to place the camera to capture the image. The points are ordered to define an optimal route for the image capture by a UAV.

An efficient route will be the set by minimizing the non-useful movement considering that the images captured by the UAV is maximised.

A point sorting algorithm has been designed in this paper. The first point of the matrix $\boldsymbol{Q_t}$ is chosen as the starting point, which is the southernmost and easternmost point of the $\boldsymbol{Q_t}$. All points that belong spatially to the first column of the $\boldsymbol{Q_t}$, ~~i.e~~i.e., all those that have the same x coordinate, are ordered in ascending ranking. Then, they are grouped in a vector, therefore, the UAV passes through all the column points consecutively from south to north. The points of the column to the right of the previous one are chosen and grouped in other vector, leading to the UAV moves all the points in an orderly way downwards, from north to south. Then, both vectors are concatenated, and the operation is repeated for the following columns alternately. That leads to the UAV passes ~~It leads ensure that the UAV passes~~ through all the points of the matrix in an orderly manner and capturing images both back and forth. The non-useful flight time is that in which the UAV will pass from the last point of a column to the first point of the next column. This approach minimised the non-useful time, reducing the total flight time, and optimised the batteries. These ordered points will be in a list with the coordinates for waypoints, and it will be sent to the UAV.

The units are necessary that will be the same to perform these calculations. However, the coordinates of the vertices of the area to be explored are usually given by a global positioning system (GPS), and the measurements of the images depend on the optical and geometric

Con formato: Resaltar
Con formato: Resaltar
Con formato: Resaltar
Con formato: Resaltar
Con formato: Resaltar
Código de campo cambiado
Con formato: Sin Resaltar
Con formato: Sin Resaltar
Código de campo cambiado
Código de campo cambiado
Código de campo cambiado
Con formato: Sin Resaltar
Con formato: Sin Resaltar
Con formato: Resaltar
Con formato: Sin Resaltar
Con formato: Sin Resaltar
Con formato: Sin Resaltar
Con formato: Sin Resaltar

characteristics of the camera, i.e. in meters. This approach converts the meters into GPS coordinates employing the Haversine formula [23].

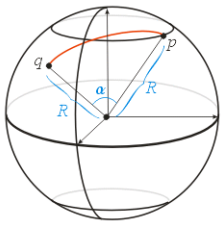

Figure 4: Distance between two points of a sphere.

The Haversine formula ~~-~~used in this approach allows to determine the shortest distance ~~leads to the approach determines the shortest distance~~ between 2 points belonging to a perfect sphere orthodromically (Figure 4~~Figure 4~~) given its longitudes and latitudes in GPS coordinates, without approximating the curvature between them. Since the Earth is a spherical flat at the poles and bulky at the equator, but with a flattening ratio of 1/298, the approximation to a sphere is accurate (with a maximum error of 0.5%). The Haversine formula is the most appropriate for short distances, but there are other mathematical methods to find orthodromic distance. The Haversine formula is expressed by equation (14):

$$haversin\left(\frac{d}{R}\right) = haversin\left(\varphi_1 - \varphi_2\right) + \cos\left(\varphi_1\right)\cos(\varphi_2) haversin\left(\lambda_1 - \lambda_2\right) \quad (14)$$

where:

- d : distance between points (in meters).
- R : radius of the sphere, i.e. the terrestrial sphere (in meters).
- φ_i latitude of point i.
- λ_i: point length i.

and the function of Haversine is defined by equation (15):

$$haversine\left(\alpha\right) = sen^2\left(\frac{\alpha}{2}\right) \quad (15)$$

Equation (16) is employed to calculate the distances between two points whose angle to the centre of the sphere is α.

$$d = \alpha \cdot R \quad (16)$$

Equations (17-19) are employed to minimize the computational costs.

Código de campo cambiado
Código de campo cambiado
Con formato: Resaltar
Código de campo cambiado
Con formato: Fuente: Sin Negrita
Código de campo cambiado
Con formato: Sin Resaltar
Código de campo cambiado
Código de campo cambiado
Con formato: Sin Resaltar
Con formato: Sin Resaltar
Con formato: Sin Resaltar
Con formato: Sin Resaltar
Con formato: Sin Resaltar
Código de campo cambiado
Con formato: Sin Resaltar
Código de campo cambiado
Con formato: Sin Resaltar
Código de campo cambiado
Con formato: Sin Resaltar

$$a = \sin^2\left(\frac{\varphi_1 - \varphi_2}{2}\right) + \cos(\varphi_1)\cos(\varphi_2)\sin^2\left(\frac{\lambda_1 - \lambda_2}{2}\right) \quad (17)$$

$$c = 2 \cdot \operatorname{atan2}\left(a^2, (1-a)^2\right) \quad (18)$$

$$d = R \cdot c \quad (19)$$

where R is the average radius of the earth, being in this case R = 6.371x10^6 m.

The results show that when two pairs of points with a similar GPS coordinate differences are taken, but with different positions on the sphere, the distance between the points of each pair is not constant. In addition, neither vertical nor horizontal distances are proportional to each other, but also depend on the GPS coordinates of each pair of points. This is due to how GPS coordinates are defined, depending on the latitude and longitude at which the point is positioned on the sphere, see Figure 5~~Figure 5~~:

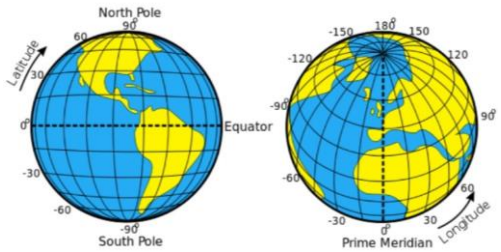

Figure 5: Latitude and Longitude

The conversion factors of GPS coordinates to meters are not constant. They must be calculated from the particular position of the reference points, considering the difference between them. The Haversine's formula is used horizontally and vertically to find the conversion factors of GPS coordinates to meters, calculating the correspondence between a degree and its distance in meters for the chosen point. For the x-axis, the conversion factor can be calculated from a reference point and other auxiliary point located at one degree horizontally. For the y-axis, it is calculated the conversion factor in a similar way, with one reference point and other located at one degree vertically. Therefore, for the horizontal and vertical distances between two points $\boldsymbol{P}_1$ and $\boldsymbol{P}_2$, it is possible to use the Haversine formula, using two auxiliary points $\boldsymbol{P}_{2x}$ and $\boldsymbol{P}_{2y}$, where: $\boldsymbol{P}_1 = (\varphi_1, \lambda_1)$, $\boldsymbol{P}_2 = (\varphi_2, \lambda_2)$, $\boldsymbol{P}_{2x} = (\varphi_2, \lambda_1)$, $\boldsymbol{P}_{2y} = (\varphi_1, \lambda_2)$. The equations (20-22) are obtained considering the previous points.

Código de campo cambiado
Código de campo cambiado
Código de campo cambiado
Con formato: Sin Resaltar
Código de campo cambiado
Con formato: Sin Resaltar
Con formato: Sin Resaltar
Código de campo cambiado
Con formato: Sin Resaltar
Código de campo cambiado
Con formato: Fuente: Sin Negrita
Código de campo cambiado
Código de campo cambiado
Código de campo cambiado
Código de campo cambiado
Código de campo cambiado
Código de campo cambiado
Código de campo cambiado
Código de campo cambiado
Código de campo cambiado

$$a_x = \sin^2\left(\frac{\varphi_1 - \varphi_2}{2}\right) \quad (20)$$

$$a_y = \cos(\varphi_1)\cos(\varphi_2)\sin^2\left(\frac{\lambda_1 - \lambda_2}{2}\right) \quad (21)$$

$$c_i = 2 \cdot \text{atan2}\left(a_i^2, (1-a_i)^2\right) \quad (22)$$

and the distances would be expressed by equations (23-24):

$$d_x = c_x \cdot R \quad (23)$$

$$d_y = c_y \cdot R \quad (24)$$

Where d_x is the horizontal distance between $\boldsymbol{P}_1$ and $\boldsymbol{P}_2$ and d_y is the vertical distance between $\boldsymbol{P}_1$ and $\boldsymbol{P}_2$

The conversion factors for the area over which the tessellation process is being carried out is calculated considering the $\boldsymbol{Q}_t$ as reference. With these factors, it is converted the dimensions of the rectangle to degrees by equations (25-26).

$$a(GPS) = \frac{a}{d_y} \quad (25)$$

$$b(GPS) = \frac{b}{d_x} \quad (26)$$

Código de campo cambiado
Código de campo cambiado
Código de campo cambiado
Con formato: Sin Resaltar
Con formato: Sin Resaltar
Con formato: Sin Resaltar
Con formato: Sin Resaltar
Con formato: Sin Resaltar
Con formato: Sin Resaltar
Con formato: Sin Resaltar
Código de campo cambiado
Con formato: Sin Resaltar
Código de campo cambiado
Con formato: Sin Resaltar
Con formato: Sin Resaltar
Código de campo cambiado
Con formato: Sin Resaltar
Código de campo cambiado
Código de campo cambiado
Con formato: Sin Resaltar
Código de campo cambiado
Código de campo cambiado
Código de campo cambiado
Con formato: Inglés (Reino Unido)
Código de campo cambiado

Figure 6: Perimeter of the polygon to be inspected. In red, the optimal route that the UAV will follow within the polygon to obtain multispectral images.

3. Flight Cycle

The maximum distance the UAV can travel is considered to set the flight cycles when the optimal route of the UAV flight has been found (done according the approach showed in Section 2).

The flight cycle is defined as the route taken by the UAV from an initial point, the points that are part of the route of the optimal route and the return to the initial point. The distance travelled must be less than the maximum distance that the UAV can flight.

The points to visit in each cycle are a subset points where the route, which is not repeated in different cycles, has the same start and end points for all cycles, chosen arbitrarily due to their proximity to the control posts. It simplifies the work of a UAV operator. Therefore, the operator chooses a point for the landing of the UAV that is more appropriate for the change of batteries, etc. [24].

Con formato: Justificado
Código de campo cambiado
Con formato: Sin Resaltar
Con formato: Sin Resaltar
Con formato: Sin Resaltar
Con formato: Sin Resaltar
Con formato: Sin Resaltar
Con formato: Sin Resaltar
Código de campo cambiado

The maximum distance is found by the maximum flight time with the battery fully charged [25]. Although it is not an exact value, the result is close to the real value. The maximum distance must be more than the distance between points of the optimal route. Possible disturbances that affect the calculation of this value are generally environmental, e.g. wind speed and direction and ambient temperature, etc. [26]. Usually, the maximum flight time is reflected in the UAV specifications, which allows a first conservative approach that can be adjusted experimentally.

The geolocation of the UAV through GPS coordinates has been considered to calculates flight cycles. These coordinates are not absolute but depend on the location of the area to be explored within the globe, and, because of maximum flight distance can be expressed in meters, the relation between the two coordinate systems is found.

A heuristic approach that requires less processing cost has been chosen referring to an arbitrary point of origin, although the exact position in meters of each point could be calculated and placed in a position matrix. The maximum distance (given in meters) is converted to a GPS coordinate differential, using the conversion factor presented by the most unfavourable scenario, i.e. the maximum between both factors. This method reduces the accuracy of the procedure but generates less computational cost.

The maximum distance between GPS coordinates will be employed in an algorithm to calculate the theoretical distance travelled by the UAV between the points of the optimal route. The distance to the first point of the route is calculated from the starting point. The accumulated distance is also calculated as it advances through the optimal route, and the instantaneous return distance and the total distance is compared with the maximum distance. The return distance is a distance that depends on the last point of the optimal route before returning to the base. In some cases, it is an important value, depending on the geometric shape of the area to be analysed and its size, or the size of the images to be captured. In addition, it is a variable value that depends on the last position. For this reason, the calculation of the distances and their verification is done at each of the points. For example, let P_s be the initial point and P_i the points within the optimal route, $i = 1, 2, 3 \ldots n$. Initially, only with P_1 (the first point) the outward distance (distance between P_s and P_1), the distance between travelled points and the return distance (distance between $\mathbf{P_1}$ and $\mathbf{P_s}$) are calculated. If the total distance is less than or equal to the maximum distance, then it continues to the next point. In the next loop, the distance travelled will be the distance between points P_1 and P_2, and the return distance will be the distance between P_2 and P_s. In the third loop, the distance between points is the

Código de campo cambiado
Código de campo cambiado
Con formato: Sin Resaltar
Con formato: Sin Resaltar
Con formato: Sin Resaltar
Código de campo cambiado
Código de campo cambiado
Código de campo cambiado
Código de campo cambiado
Con formato: Sin Resaltar
Código de campo cambiado
Con formato: Sin Resaltar
Código de campo cambiado
Con formato: Sin Resaltar
Código de campo cambiado
Código de campo cambiado
Código de campo cambiado
Código de campo cambiado

accumulated distance: distance between P_1 and P_2 plus the distance between P_2 and P_3, and the return distance will be the distance between P_3 and P_s.

If the distance is less than the maximum distance, the points are saved in a vector that will define the cycle. If the distance is greater, the cycle is defined with the vector of accumulated points, the vector is stored in a matrix for later use, the cycle counter is increased, and the current position is saved as the start of the next cycle.

4. Conclusions

An algorithm has been developed to manage unmanned automatic vehicles (UAV) routes efficiently focused on multispectral imaging. The objective is to acquire multispectral images to be subsequently joined to create a larger image. This method ensures that the UAV travel the maximum distance, according to the parameters of the camera. The input data are the vertices of an irregular polygon that forms the area. A field of view and a specific height will be obtained regarding to the parameters of the camera and the desired ground distance sample.

A solution has been developed for interruptions in the inspection of large areas due to the limitations of UAV batteries. An algorithm has been created that dynamically checks the maximum points it can travel based on the characteristics of the flight, battery, distance between points, etc. It allows as many autonomous missions as necessary to be generated independently. It has been designed in such a way that the UAV returns to the starting point between the different missions. It leads that the operator can change the batteries and continue with the next flight. This novel intelligent management approach for agricultural purposes leads to enhance precision agriculture, as well as minimize production costs and manage crops in an efficient manner. The approach considers the following restrictions for multispectral images: Have a common area (in %) in both x and y directions to join the images; Perform the least number of waypoints; Travel odd rows in one direction and even rows in another to optimize the flight, etc ;Move in a straight line between the end of row points and start of the next to optimize the route.

Acknowledges

The work reported herewith has been financially by the Dirección General de Universidades, Investigación e Innovación of Castilla-La Mancha, under Research Grant (Ref.: SBPLY/19/180501/000102).

Código de campo cambiado
Código de campo cambiado
Código de campo cambiado
Código de campo cambiado
Código de campo cambiado
Código de campo cambiado

Con formato: Sin Resaltar

References

1. de Janvry, A.; Sadoulet, E. How experimental research in agriculture has gone from lab to field. *World Development* **2020**, *127*, 104782.
2. Lee, S. Role of social and solidarity economy in localizing the sustainable development goals. *International Journal of Sustainable Development & World Ecology* **2020**, *27*, 65-71.
3. Borlu, Y.; Glenna, L. Environmental concern in a capitalist economy: Climate change perception among us specialty-crop producers. *Organization & Environment* **2020**, 1086026619897545.
4. Zaman, N.; Seliaman, M.E.; Hassan, M.F.; Márquez, F.P.G. *Handbook of research on trends and future directions in big data and web intelligence*. Information Science Reference: 2015; Vol. 1, p 253-265.
5. Klerkx, L.; Rose, D. Dealing with the game-changing technologies of agriculture 4.0: How do we manage diversity and responsibility in food system transition pathways? *Global Food Security* **2020**, *24*, 100347.
6. Pliego Marugán, A.; García Márquez, F.P. Advanced analytics for detection and diagnosis of false alarms and faults: A real case study. *Wind Energy* **2019**, *22*, 1622-1635.
7. Márquez, F.P.G.; Muñoz, J.M.C. A pattern recognition and data analysis method for maintenance management. *International Journal of Systems Science* **2012**, *43*, 1014-1028.
8. Pedregal, D.J.; García, F.P.; Roberts, C. An algorithmic approach for maintenance management based on advanced state space systems and harmonic regressions. *Annals of Operations Research* **2009**, *166*, 109-124.
9. Márquez, F.P.G.; Pedregal, D.J. Applied rcm 2 algorithms based on statistical methods. *International Journal of Automation and Computing* **2007**, *4*, 109-116.
10. García Márquez, F.P.; García-Pardo, I.P. Principal component analysis applied to filtered signals for maintenance management. *Quality and Reliability Engineering International* **2010**, *26*, 523-527.
11. Pliego Marugán, A.; García Márquez, F.P.; Lev, B. Optimal decision-making via binary decision diagrams for investments under a risky environment. *International Journal of Production Research* **2017**, *55*, 5271-5286.
12. Pliego, A.; Márquez, F.P.G. Big data and web intelligence: Improving the efficiency on decision making process via bdd. In *Big data: Concepts, methodologies, tools, and applications*, IGI Global: 2016; pp 229-246.

Código de campo cambiado

13. Márquez, F.P.G.; Pardo, I.P.G.; Nieto, M.R.M. Competitiveness based on logistic management: A real case study. *Annals of Operations Research* **2015**, *233*, 157-169.

14. Herraiz, Á.H.; Marugán, A.P.; Ramirez, I.S.; Papaelias, M.; Márquez, F.P.G. Remotely operated vehicle applications. In *Non-destructive testing and condition monitoring techniques for renewable energy industrial assets*, Elsevier: 2020; pp 119-132.

15. Marquez, F.G. An approach to remote condition monitoring systems management. *IET* **2006**, *1*, 156-160.

16. Segovia, I.; Pliego, A.; Papaelias, M.; Márquez, F.P.G. In *Optimal management of marine inspection with autonomous underwater vehicles*, International Conference on Management Science and Engineering Management, 2019; Springer: pp 760-771.

17. Zheng, C.; Li, L.; Xu, F.; Sun, F.; Ding, M. Evolutionary route planner for unmanned air vehicles. *IEEE Transactions on robotics* **2005**, *21*, 609-620.

18. Márquez, F.P.G.; Ramírez, I.S. Condition monitoring system for solar power plants with radiometric and thermographic sensors embedded in unmanned aerial vehicles. *Measurement* **2019**, *139*, 152-162.

19. Ramírez, I.S.; Marugán, A.P.; Márquez, F.P.G. In *Remotely piloted aircraft system and engineering management: A real case study*, International Conference on Management Science and Engineering Management, 2018; Springer: pp 1173-1185.

20. Muñoz, C.Q.G.; Gonzalo, A.P.; Ramirez, I.S.; Márquez, F.P.G. In *Online fault detection in solar plants using a wireless radiometer in unmanned aerial vehicles*, International conference on management science and engineering management, 2017; Springer: pp 1161-1174.

21. Ma, T.; Li, P.; Ma, T. A three-dimensional cartesian mesh generation algorithm based on the gpu parallel ray casting method. *Applied Sciences* **2020**, *10*, 58.

22. Wu, W.-Y. Dominant point detection using adaptive bending value. *Image and Vision Computing* **2003**, *21*, 517-525.

23. Chopde, N.R.; Nichat, M. Landmark based shortest path detection by using a* and haversine formula. *International Journal of Innovative Research in Computer and Communication Engineering* **2013**, *1*, 298-302.

24. Moraleda, V.B.; Marugán, A.P.; Márquez, F.P.G. In *Acoustic maintenance management employing unmanned aerial vehicles in renewable energies*, International Conference on Management Science and Engineering Management, 2018; Springer: pp 969-981.

25. Segovia Ramírez, I.; Bernalte Sánchez, P.J.; Papaelias, M.; García Márquez, F.P. In *Autonomous underwater vehicles inspection management: Optimization of field of view and measurement process*,

13th International Conference on Industrial Engineering and Industrial Management, 2019; Servicio de Publicaciones de la Universidad de Oviedo.

26. Muñoz, C.Q.G.; Jiménez, A.A.; Márquez, F.P.G. Wavelet transforms and pattern recognition on ultrasonic guides waves for frozen surface state diagnosis. *Renewable Energy* **2018**, *116*, 42-54.